Journal of Civil and Hydraulic Engineering
https://www.acadlore.com/journals/JCHE

Assessment of Fatigue Life in H-Type Bridge Hangers Subjected to Torsional Vibration

Yuyang Sun*, Zhouyuan Xu, Zhihao Wang

School of Civil Engineering and Communication, North China University of Water Resources and Electric Power, 450011 Zhengzhou, China

* Correspondence: Yuyang Sun (543061893@qq.com)

Received: 05-08-2024 **Revised:** 07-01-2024 **Accepted:** 07-10-2024

Citation: Y. Y. Sun, Z. Y. Xu, and Z. H. Wang, "Assessment of fatigue life in H-type bridge hangers subjected to torsional vibration," *J. Civ. Hydraul. Eng.*, vol. 2, no. 3, pp. 131–141, 2024. https://doi.org/10.56578/jche020301.

Abstract: The fatigue life of H-type rigid hangers, crucial components in bridge engineering, is investigated in this study, particularly under the influence of torsional vibrations induced by wind loads. These hangers, integral to the integrity and longevity of bridge structures, are characterized by their high aspect ratio and low torsional stiffness, which predispose them to fatigue under such conditions. The focus of the research is the hangers of Dongping Bridge, located in Foshan, Guangdong. Through the application of theoretical analysis and finite element simulation using ABAQUS, the effects of bolting actions were simulated using connector elements, which enhanced computational efficiency and facilitated the stress analysis at the bolt holes in node plates. Furthermore, fe-safe fatigue analysis software was utilized to evaluate the fatigue life, adhering to established guidelines. The findings reveal that selecting an appropriate stiffness for the connector elements is critical in accurately simulating the bolting action. It was determined that the torsional amplitude at mid-span is a viable indicator for assessing fatigue damage. A torsional vibration control threshold of 6.25° is recommended for hangers measuring 40.212 meters in length.

Keywords: Structural fatigue; Finite element simulation; H-type hangers; Torsional vibration; Fatigue analysis software

1 Introduction

H-type rigid hangers, often non-streamlined blunt section members [1, 2], are prone to wind-induced torsional vibrations due to their large aspect ratio, low damping, and poor aerodynamic stability [3, 4]. Inadequate design can lead to fatigue accumulation and failure, posing risks to safety and property [5–10]. Instances such as the Fire Island Bridge [11, 12] in the USA and the Dongping Bridge in China highlight the severity of such issues. Since the concept of fatigue was introduced in the 19th century [13], the S-N curve methodology has become a mainstay in bridge design codes worldwide for assessing hanger fatigue life [14–17]. International standards address such fatigue issues [18–20], including the British Standard BS5400, the American AASHTO Standard, the European Eurocode 3, and the Specification for Design of Highway Steel Bridges. Beyond stress, stress levels significantly influence the fatigue life of structures, necessitating stress correction under varying yield levels to ensure accuracy in fatigue life assessment. Typically, the Gerber correction is applied for brittle materials and the Goodman curve [21] correction for ductile materials in engineering practices. With advancements in computer technology, finite element simulation software like ABAQUS, ANSYS, and MIDAS have been applied to engineering problems [22–24]. The judicious use of finite element software simplifies complex engineering issues. fe-safe, as a fatigue analysis software [25, 26], features advanced algorithms and comprehensive functionality, effectively facilitating fatigue analysis in conjunction with finite element methods [27, 28].

This paper validates the accuracy of the finite element model and examines the impact of bolt action on H-type members using connector elements. It studies the effect of bolt quantity and arrangement on torsional impact, assessing fatigue life at different torsional angles using international codes and fe-safe software, thereby establishing torsional vibration standards for H-type hangers considering fatigue.

2 Theoretical Calculation Method and Finite Element Model Establishment for H-type Hangers

Under the action of torque, non-circular cross-section members experience warping, where the cross-section no longer remains planar, and points on the section undergo axial displacement. This phenomenon is known as warping. Torsion in members is categorized into free torsion and restrained torsion. Free torsion occurs under the action of torque couples at both ends without any warping constraints, characterized by uniform warping across sections, unchanged longitudinal fiber lengths, and the presence of only shear stress without normal stress on the cross-section. Conversely, restrained torsion, influenced by constraints, leads to varying degrees of warping across sections, changes in longitudinal fiber lengths between adjacent sections, and results in bending deformation of the member, generating both normal and shear stresses on the cross-section.

The H-shaped section, being bilaterally symmetrical, has its shear center coinciding with the centroid. The web plate passing through the shear center remains unwarping, while warping occurs in the upper and lower flanges. Figure 1 shows the schematic diagram of the H-shaped rod under torsion. According to AISC's Steel Design Guide 9 [29, 30], the calculation method for the torsional angle of a member subjected to concentrated torsion at fixed ends is as follows:

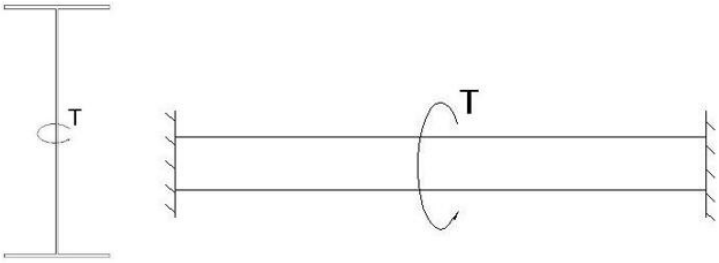

Figure 1. Schematic diagram of member torsion

$$0 \le z \le \alpha l:$$

$$\theta = \frac{Ta}{(H+1)\mathrm{GJ}} \left\{ \left[H \times \left(\frac{1}{\sinh \frac{l}{a}} + \sinh \frac{\alpha l}{a} - \frac{\cosh \frac{\alpha l}{a}}{\tanh \frac{l}{a}} \right) + \left(\sinh \frac{l}{a} - \frac{\cosh \frac{\alpha l}{a}}{\tanh \frac{l}{a}} + \frac{1}{\tanh \frac{l}{a}} \right) \right] \times \left(\cosh \frac{z}{a} - 1 \right) - \sinh \frac{z}{a} + \frac{z}{a} \right\}$$

$$\alpha l \le z \le l:$$

$$\theta = \frac{Ta}{\left(\frac{1}{H}+1\right)\mathrm{GJ}} \left[\left(\frac{\cosh \frac{\alpha l}{a} - 1}{H \times \sinh \frac{l}{a}} + \frac{\cosh \frac{\alpha l}{a} - \cosh \frac{l}{a} + \frac{l}{a} \times \sinh \frac{l}{a}}{\sinh \frac{l}{a}} \right) + \cosh \frac{z}{a} \left(\frac{1 - \cosh \frac{\alpha l}{a}}{H \times \tanh \frac{l}{a}} + \frac{1 - \cosh \frac{\alpha l}{a} \times \cosh \frac{l}{a}}{\sinh \frac{l}{a}} \right) + \sinh \frac{z}{a} \left(\frac{\cosh \frac{\alpha l}{a} - 1}{H} + \cosh \frac{\alpha l}{a} \right) - \frac{z}{a} \right]$$

where:

$$H = \frac{\frac{1-\cosh \frac{\alpha l}{a}}{\tanh \frac{l}{a}} + \frac{\cosh \frac{\alpha l}{a}-1}{\sinh \frac{l}{a}} + \sinh \frac{\alpha l}{a} - \frac{\alpha l}{a}}{\frac{\cosh \frac{l}{a}+\cosh \frac{\alpha l}{a} \times \cosh \frac{l}{a}-\cosh \frac{\alpha l}{a}}{\sinh \frac{l}{a}} + \frac{l}{a}(\alpha - 1) - \sinh \frac{\alpha l}{a}}$$

T-Concentrated torque.
z-Along the axis of the member, calculate the distance from the cross-section to the left support section.
αl-The distance from the section where the concentrated torque is applied to the left support section.
G-Material shear modulus.
I_ω-Section warping constant, for H-type section $I_\omega = \frac{I_y h^2}{4}$.
h-The total height of the section minus the thickness of one flange.
$\mathrm{I_y}$-Moment of inertia about the weak axis.
J-Section torsional constant, with an approximate calculation method of $J \approx \sum \left(\frac{bt^3}{3} \right)$.
$\mathrm{b_f}$-Flange width; $\mathrm{b_w}$-Web width; $\mathrm{t_s}$-Web thickness; $\mathrm{t_w}$-Flange thickness.
The warping normal stress of the flange plate can be expressed as: $\sigma = E\omega_{ns}\theta''$.
ω_{ns}-Warping function $\omega_{ns} = \frac{hb_f}{4}$.

θ''-the second derivative of θ with respect to z.

Employing the previously delineated calculation method and considering the geometric dimensions of Dongping Bridge's Rod No. 1, the calculations under fixed boundary conditions reveal that applying a concentrated torque of 100 N·m at mid-span results in a maximum torsional angle of θ=9.835×10^{-4} rad and a peak normal stress of σ=4.64×10^{-1} MPa.

In the finite element analysis, planar shell elements within the shell element category are utilized to construct the flange and web parts of the member, replicating the actual bridge dimensions. The web, devoid of perforations, is defined in terms of shell thickness within the properties section. Assembly and merging of the flange and web are conducted through the assembly module, creating a general static analysis step. Due to the absence of a fixed unit system in ABAQUS, appropriate units are selected, in this case, mm, N, and MPa. A reference point is established at the shear center of the mid-span section's cross-section. This reference point is coupled with the mid-span section in the interaction module's constraint creation part. The torque applied to this reference point in the load module is quantified as 10^5 (100 N·m). Boundary conditions entail complete fixation of both ends' sections (U1=U2=U3=UR1=UR2=UR3=0), and the mesh primarily consists of quadrilateral divisions. The calculation results are shown in Figure 2: maximum torsional angle θ=9.994×10^{-4} rad normal stress σ=4.633×10^{-1} MPa. The error in torsional angle is approximately 1.62%, and that in normal stress is around 0.15%, affirming the finite element model's accuracy and laying the groundwork for further research.

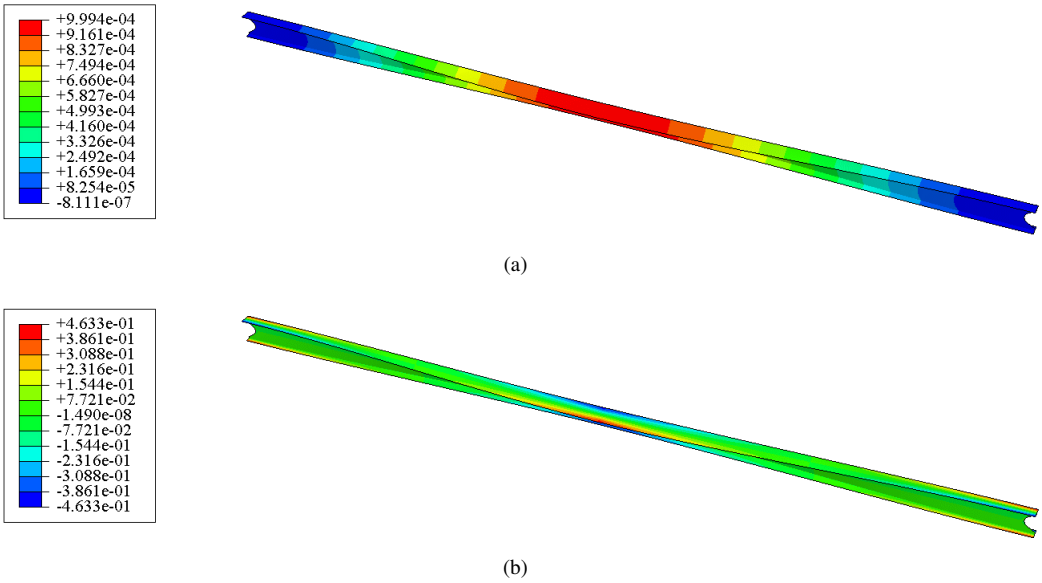

Figure 2. Torsion diagram (a) normal stress diagram (b)

3 Simulation of Contact Relationships

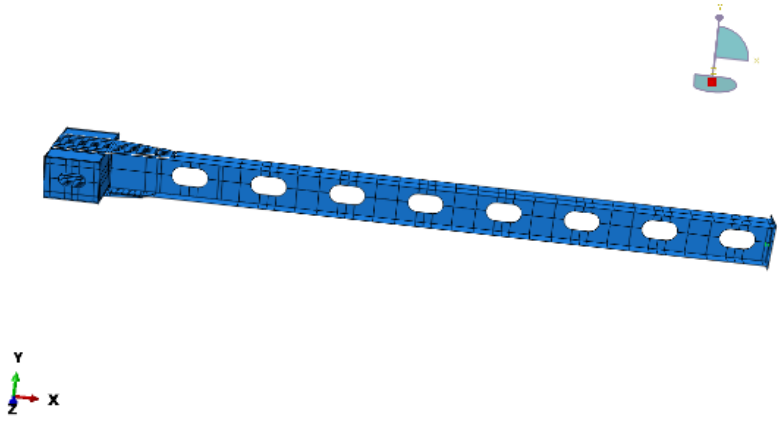

Figure 3. Assembly diagram of the connection cross-ssection stiffness fitting model

The finite element simulation primarily focuses on the emulation of bolted contact at the node plates. In this context, a tie rod box model, with dimensions matching those used in engineering, is established in ABAQUS, and the base of the tie rod box is fixed. For simulating the contact relationship between the node plate and the tie rod box, two approaches are employed: 1. Following the parameters from "Rigid Slender Hangers in Steel Arch Bridges: Wind-Induced Vibrations, Fatigue, and Control," the bolted connection behavior between the hanger flange and the node plate is simplified using surface-to-surface contact constraints, adopting 8500 N/mm as the contact stiffness. 2. Connector elements are selected to simulate the bolted contact at the node plate. Numerical simulations are carried out using experimental components similar to the project, with connector element stiffness fitted accordingly. The components used are H-shaped steel with web openings, and the boundary condition involves bolting one end of the flange plate to the reaction box through the node plate, creating a cantilever condition, and applying concentrated torque at the other end. Refer to Figure 3 for the assembly diagram.

The model is subjected to the same 2.71 kN·m torque as in reference [5], with dimensions consistent with the experimental components. In the modeling, the concentrated torque is applied to a rigid plate, which is then coupled with the cantilever end to prevent stress concentration during loading.

Different stiffnesses of connector elements are tested under the given torque. In the experiment, when 2.71 kN·m torque is applied, the cantilever end's torsional angle is 9.3°. The calculated torsional angles under different connector element stiffness scenarios are summarized in the following table. When the connector element stiffness is set to 805 N/mm, the torsional angle is 9.299°, closely matching the experimental result. The finite element model's maximum normal stress is 80.93 MPa, as shown in the stress distribution diagram. In the experiment, the maximum normal stress at the cantilever end is 72.6 MPa, compared to 71.92 MPa in the same location in the finite element model. The maximum normal stress at the node plate in the experiment is 73.05 MPa, versus 72.13 MPa in the finite element model, with errors of 0.85% and 1.27%, respectively. It is concluded that this stiffness level adequately simulates the contact action at the node plate. The calculation results under different stiffnesses are shown in Table 1, and the stiffness fitting curve is shown in Figure 4.

Table 1. Connector element stiffness fitting table

Working Condition	Stiffness N/mm	Rotational Angle°
Working Condition 1	100	10.325
Working Condition 2	500	9.683
Working Condition 3	800	9.305
Working Condition 4	805	9.299
Working Condition 5	850	9.248
Working Condition 6	1000	9.081

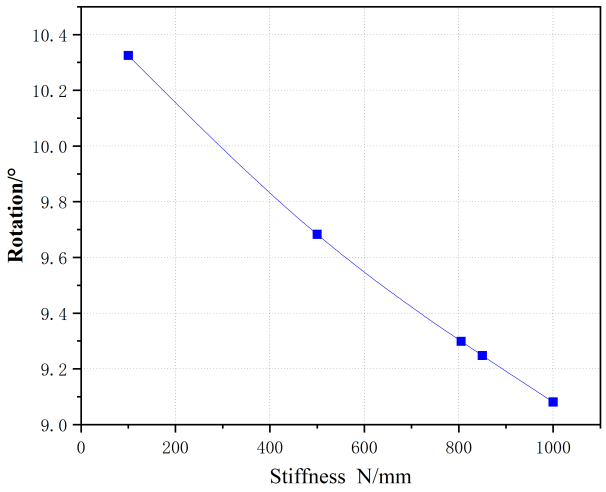

Figure 4. Connector element stiffness fitting chart

4 The Impact of Bolts on the Torsion of Members

To investigate the impact of bolts on the torsional behavior of members, models of various lengths of rods from Dongping Bridge were established. These models incorporated both fixed and simulated bolted boundary

conditions. By comparing the outcomes of these two conditions, the influence coefficient of bolts on member torsion was deduced. Torsional behavior of the hangers was simulated using both torque and displacement methods, setting the torque magnitude to 1e7(10kN·m). When simulating torsion through displacement, the shear center of the mid-span cross-section was also designated as a reference point and coupled with the mid-span section, applying a torsional angle of 0.1 rad to the reference point.

Eight different lengths of members from Dongping Bridge were constructed without web openings, including rigid boundary conditions and conditions simulating bolted connections through contact stiffness (connector elements were established only for Rod No. 1 for comparative validation). Following the aforementioned simulation approach, the resulting influence coefficient (a ratio of strain or stress under bolted boundary conditions to fixed boundary conditions) was obtained. The calculation results are shown in Tables 2 and 3, and the fitting diagram of the influence coefficient is shown in Figure 5. Under a fixed torque, when the length of the member is short, the influence coefficient is relatively high, and it decreases continuously as the length of the member increases, reaching about 2.1 when the length is around 40 meters. Under a fixed rotational angle, the maximum normal stress ratio, considering bolt action and fixed boundary conditions, was around 0.6.

Table 2. Table of torsion influence coefficient table (unit: rad)

Member	Fixed	Contact Stiffness 8500/mm	Contact Element 805 N/mm	Bolt/Fixed
1	0.09994	0.212	0.21	2.12
2	0.09578	0.2086		2.18
3	0.08362	0.1837		2.20
4	0.06527	0.1501		2.30
5	0.04366	0.1071		2.45
6	0.02291	0.06106		2.67
7	0.007585	0.02272		3.00
8	0.000703	0.006525		9.28

Table 3. Table of stress influence coefficient table (unit: MPa)

Member	Fixed	Contact Stiffness 8500/mm	Bolt/Fixed
1	46.36	27.77	0.60
2	47.835	30.16	0.63
3	52.9	32.75	0.62
4	63.35	38.74	0.61
5	84.5	50.92	0.60
6	132.75	78.64	0.59
7	282	162.8	0.58

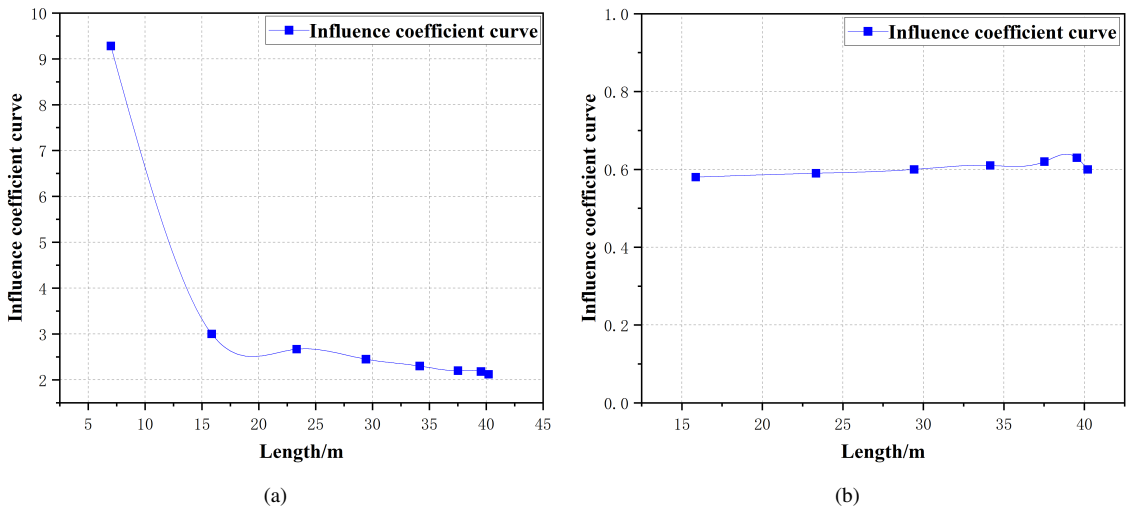

Figure 5. Trend graph of influence coefficients: Rotational angle (a), Stress (b)

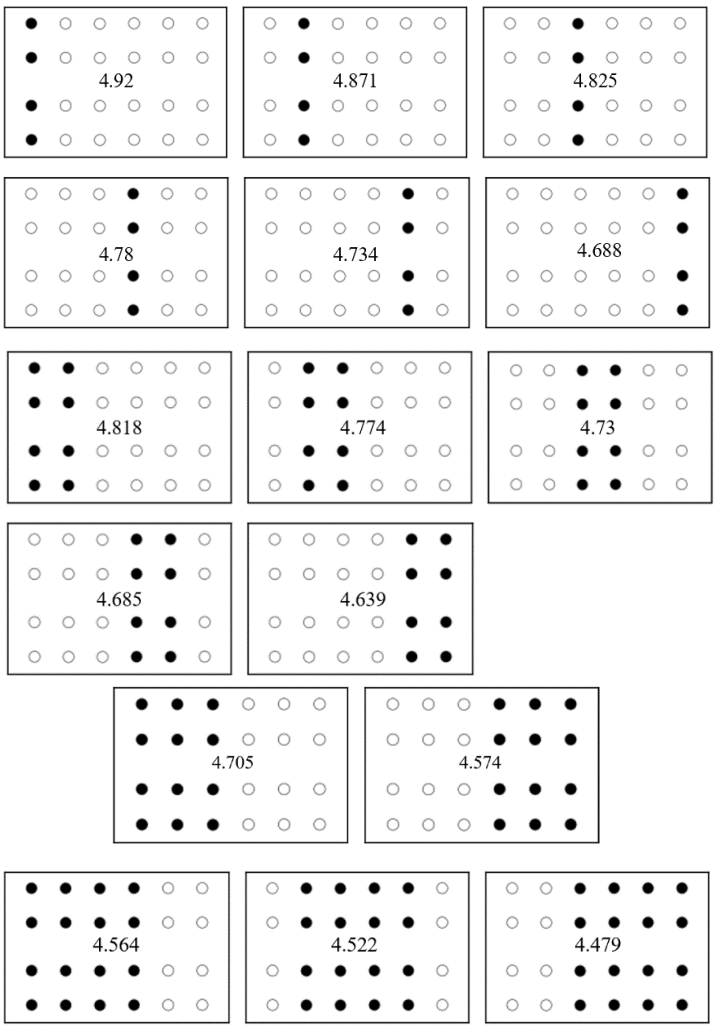

Figure 6. Comparison of torsional angles at different layout positions

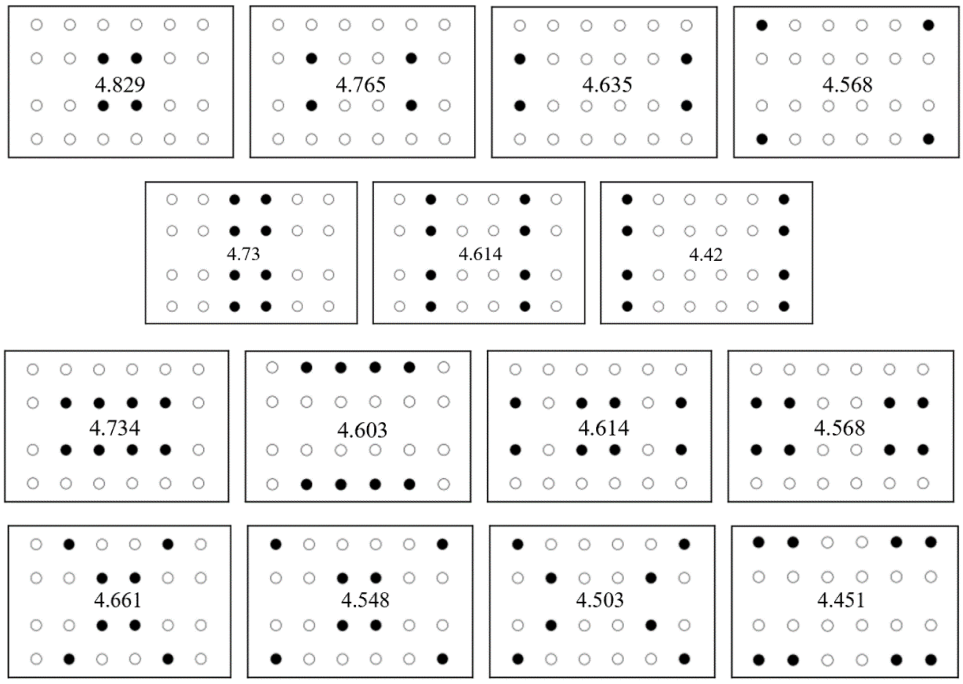

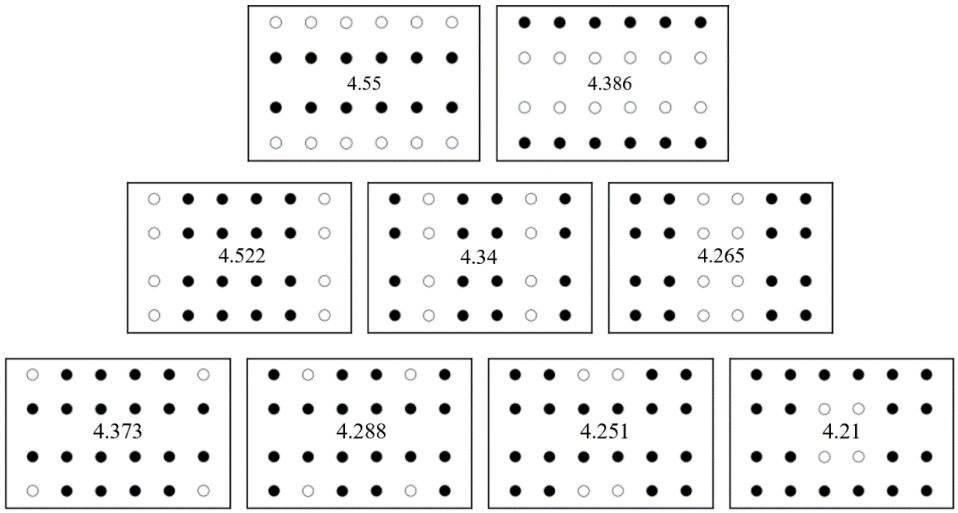

Figure 7. Torsional angles of members under conditions of colts with varying degrees of dispersion

In order to further investigate the impact of bolts on the torsion of members, a study was conducted in ABAQUS by varying the number and arrangement of bolts at the node plates, applying the same magnitude of torque, and comparing the resulting strain outcomes.

The flange plate bolt count was set at 4, 6, 8, 12, 16, 18, 20, and 24, with a torque magnitude of 100N·m applied. Comparing torsional angles yielded the following primary patterns:

To further investigate the effects of bolt quantity and arrangement on the torsional response, the study systematically varied the configuration of bolts at the node plates under specified torque, observing the resulting torsional angles. For the initial group with four bolts, varying arrangements across six columns were examined, revealing torsional angles from 4.92 to 4.688 ($\times 10^{-3}$ rad) for different setups. Subsequent tests with eight, twelve, and sixteen bolts, distributed across specified column combinations, showed a decrease in torsional angles, illustrating that closer placement to the torsional load enhances torsional restraint. The specific bolt layout and calculation results are shown in Figure 6.

With consistent bolt quantity and central positioning, altering the bolt arrangement while applying a concentrated torque of 100N·m yielded comparative analysis results (in units of 10^{-3} rad). The analysis of seven groups, maintaining consistent bolt quantity and central positioning but varying in arrangement, demonstrated that each group exhibited smaller torsional angles when bolts were placed closer to the edges of the area. From these findings, it is inferred that within a certain area, dispersing bolts with consistent quantity and central positioning favors the constraint on member torsion. The specific bolt layout and calculation results are shown in Figure 7.

5 Fatigue Life Assessment

To examine the fatigue issues associated with wind-induced torsional vibrations in hangers, calculations were carried out in accordance with the fatigue sections of domestic and international standards. These standards provide fatigue limits for specific structural details. Integrating the finite element analysis of hanger torsion, a relationship between torsional angle and fatigue limit was established. Taking the Specification for Design of Highway Steel Bridges (JTG D64-2015) as an example, the fatigue detail at mid-span is rated at 160, and at the node plate at 90. Finite element results indicate that the stress amplitude at the node plate is lower than at mid-span, necessitating separate fatigue life assessments for both areas. The fatigue strength curve and equation as per the Specification for Design of Highway Steel Bridges (JTG D64-2015) are as follows:

$$\Delta\sigma_R^m N_R = \Delta\sigma_C^m \times 2 \times 10^6 \quad \left(N_R \le 5 \times 10^6, m = 3\right)$$
$$\Delta\sigma_R^m N_R = \Delta\sigma_D^m \times 5 \times 10^6 \quad \left(5 \times 10^6 \le N_R \le 10^8, m = 5\right)$$
$$\Delta\sigma_R = \Delta\sigma_L = \left(\frac{5}{100}\right)^{0.2} \Delta\sigma_D \approx 0.549\Delta\sigma_D$$

where: $\Delta\sigma_D = \left(\frac{2}{5}\right)^{\frac{1}{3}} \Delta\sigma_C \approx 0.737\Delta\sigma_C$.

In ABAQUS, different torsional amplitudes were applied to the members to assess fatigue life at the node plate and mid-span based on their stress amplitudes. The results, shown in the table below, indicate that as the torsional angle increases, the fatigue life of the members progressively decreases. The control target for torsional amplitude

at the node plate is ±6.25°, and at mid-span, it is 11.16°. Taking the lesser value, when the torsional angle of the member is less than ±6.25 degrees, the stress amplitude at both the node plate and mid-span remains below the constant amplitude fatigue limit set by the standards, indicating no fatigue failure in the hangers.

The odb file from ABAQUS was imported into fe-safe for fatigue life assessment. Material selection and corresponding S-N curve settings were analyzed, and the results are displayed in the following Figures 8 and 9. The maximum life was set at 50 million cycles, with areas exceeding 50 million cycles showing a fatigue life of 50 million cycles. At a torsional angle of 6.20°, the shortest fatigue life was found at the bolt holes of the first row of node plates, approximately $10^{6.701}$ (5 million) cycles, with an error margin of about 2% compared to the standard calculations, which is fundamentally consistent.

Using Rod No. 1 as a prototype, the study altered the length of the member to assess the fatigue life of hangers under torsional stress, with results shown in the following Table 4. It was found that for longer member lengths, fatigue issues appeared earlier at the node plates, while for shorter member lengths, fatigue issues occurred sooner at mid-span. The control objectives for torsion amplitude of different length members are shown in Figure 10.

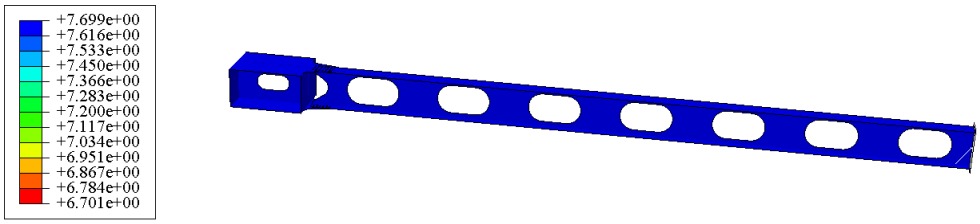

Figure 8. Overall hanger fatigue life diagram

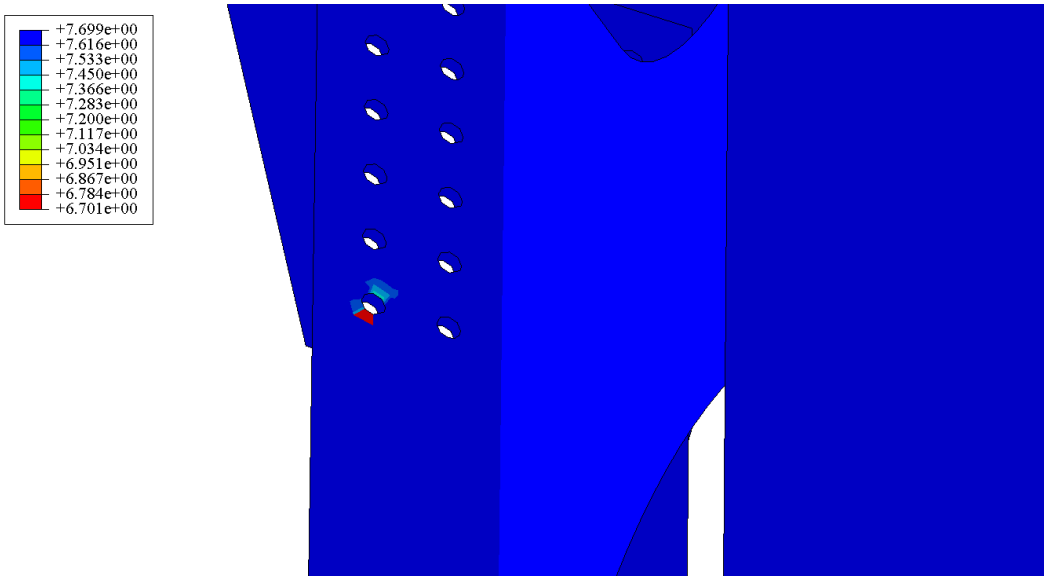

Figure 9. Location with the shortest fatigue life

Table 4. Fatigue life assessment table for hangers of different lengths

Length (m)	Torsional Amplitude Control Objective (°)	Stress Amplitude (MPa)	
		Node Plate	Mid-Span
40.2	6.20	33	36.59
34.6	5.23	33	40.62
29	4.31	33	45.68
23.4	3.43	33	54.37
17.8	2.35	27	59
12.2	1.13	18.21	59
6.6	0.37	7.49	59

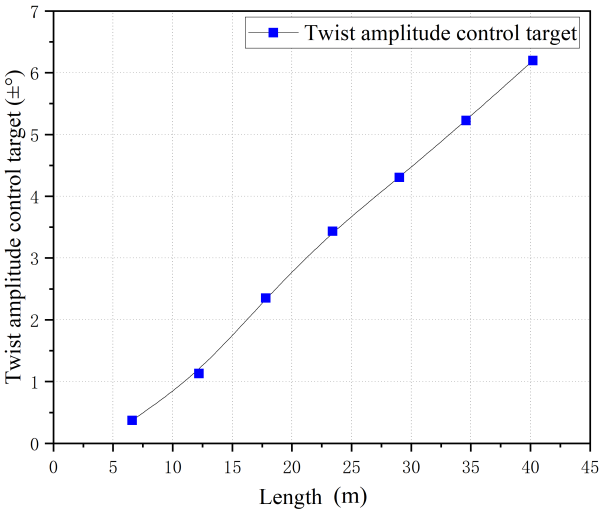

Figure 10. Fatigue life assessment for hangers of different lengths

During the finite element analysis of ABAQUS, mesh generation is an important step. The quality of the mesh directly affects the accuracy and computational efficiency of the analysis results, especially for the node plate of the H-shaped hanger in this article. Due to the presence of many bolt holes and complex structures in this area, reasonable mesh generation is crucial for the accuracy of the results. In order to ensure accuracy, the mesh needs to be sufficiently detailed to capture the stress or strain gradient in the area of interest, especially in areas of stress concentration. Excessive elements may lead to inaccurate results, while too few elements can significantly increase computational time and resource consumption. To avoid inaccurate results or waste of computational resources due to unreasonable mesh generation, different mesh sizes were used for the finite element model of the No. 1 hanger of the large-span steel arch bridge with the same remaining settings, and the results were compared. The maximum principal stress values at the first row of bolt holes and the mid-span were compared, and the maximum principal stress at the hanger node plate under different mesh sizes is shown in Table 5. When the mesh size is less than 40mm, the stress values decrease significantly as the mesh increases, and the differences between the maximum principal stress at the node plate and the mid-span are 14.79% and 35.58% at mesh sizes of 15mm and 40mm, respectively. When the mesh size is greater than 40mm, the sensitivity of the stress values at the node plate and mid-span to the mesh is relatively small, and the differences in stress values between different mesh sizes are within 10%. Based on the above results, the mesh size for the hanger model was taken as 45mm.

The fatigue life of the No. 1 suspender of the long-span steel arch bridge was evaluated according to national standards, and the torsion amplitude when reaching the constant amplitude fatigue limit in each standard was used as the control target. The specific evaluation results are shown in Table 6.

Table 5. Mesh sensitivity analysis

Mesh/(mm)	Maximum Principal Stress at the Node Plate/(MPa)	Maximum Principal Stress at Mid-Span/(MPa)
15	34.23	43.67
30	31.29	37.04
35	29.82	35.9
40	29.85	32.21
45	29.91	34.39
60	29.93	33.03
90	30.05	33.51

Table 6. Relationship between fatigue stress of derrick and torsion angle

Specification	Fatigue Level	Constant Amplitude Fatigue Limit /(MPa)	Fatigue Life	Twist Angle Limit /(°)
BS5400	C	78	10^7	±7.32
AASHTO	C	69	2×10^6	±6.48
Eurocode	90	66	5×10^6	±6.2
JTG D64-2015	90	66	5×10^6	±6.2

In addition to stress amplitude, the level of stress also impacts the fatigue life of structures. In engineering practice, the Goodman empirical formula is often used for fatigue correction in ductile materials. The equation for this formula is:

$$\sigma_a = \sigma_{-1}\left(1 - \frac{\sigma_m}{\sigma_b}\right)$$

where: σ_a-Fatigue limit amplitude.

σ_{-1}-Fatigue limit under symmetric cycling.

σ_m-Mean stress.

σ_b-Tensile strength.

In ABAQUS, different analysis steps were set for axial force and torsional angle, with the axial force being 2150 kN. The axial force was considered a constant load, assigned a coefficient of 1 in fe-safe, while the torsional load was applied as ±1. The evaluation algorithm used was Normalstress-Goodman. Fatigue life assessment based on various torsional angles indicated that at 4.46°, the fatigue life of the member is approximately 5 million cycles. Therefore, it is concluded that 4.46° can serve as the torsional amplitude control target under the influence of axial force.

6 Conclusions

1. In the finite element model, connector elements effectively simulate the bolted connection between node plates and tie rod boxes. When appropriate stiffness is selected, the stress distribution during torsion closely aligns with experimental results documented in the literature.

2. Using Dongping Bridge's hangers as a case study, the impact coefficient of bolts on the torsional angle of members decreases with increasing member length. For a 40.212m hanger, the impact coefficient is approximately 2.12; under the rotational effect, the stress impact coefficient for hangers of different lengths is around 0.6.

3. With identical numbers and arrangements, the closer the group of bolts is to the torsion end, the more effective the constraint on torsion.

4. For the same number of bolts with the central position unchanged, a more dispersed bolt distribution results in a better constraint on the torsion of the member.

5. According to fatigue life assessment methods in relevant standards, controlling the torsional angle of the central cross-section of H-type hangers can prevent fatigue failure. For Rod No. 1 of Dongping Bridge, a torsional amplitude of 4.46° can be set as the vibration control target.

Data Availability

The data supporting our research results are under privacy or ethical restrictions. The data are available from [Yuyang Sun, 543061893@qq.com] for researchers, who meet the criteria for accessing confidential data.

Conflicts of Interest

The authors declare that they have no conflicts of interest.

References

[1] C. C. Ulstrup, "Aerodynamic lessons learned from individual bridge members," *Ann. N. Y. Acad. Sci.*, vol. 352, no. 1, pp. 265–281, 1980. http://doi.org/10.1111/j.1749-6632.1980.tb16377.x

[2] Y. Nakamura, "Bluff-body aerodynamics and turbulence," *J. Wind Eng. Ind. Aerodyn.*, vol. 49, no. 1–3, pp. 65–78, 1993. http://doi.org/10.1016/0167-6105(93)90006-A

[3] Y. C. Deng, S. Y. Li, and Z. Q. Chen, "Unsteady theoretical analysis on the wake-induced vibration of suspension bridge hangers," *J. Bridge Eng.*, 2019. https://doi.org/10.1061/(ASCE)BE.1943-5592.0001339

[4] P. Hémon, F. Santi, B. Schnoerringer, and J. Wojciechowski, "Influence of free-stream turbulence on the movement-induced vibrations of an elongated rectangular cylinder in cross-flow," *J. Wind Eng. Ind. Aerodyn.*, vol. 89, no. 14, 2001. https://doi.org/10.1016/S0167-6105(01)00126-X

[5] P. Keller, C. Higgins, and S. C. Lovejoy, "Evaluation of torsional vibrations in steel truss bridge members," *J. Bridge Eng.*, vol. 20, no. 9, pp. 1–10, 2015. https://doi.org/10.1061/(ASCE)BE.1943-5592.0000688

[6] Y. Kubo, K. Sakurai, and S. Azuma, "Aerodynamic characteristics of H-shaped section cylinder in laminar and turbulent flows," *Memo. Kyushu Inst. Technol. Eng.*, vol. 10, pp. 1–13, 1980.

[7] Y. S. Song, Y. L. Ding, W. Zhong, and H. W. Zhao, "Fatigue-life assessment of short steel hanger in a rigid tied arch bridge integrating multiple factors," *J. Perform. Constr. Facil.*, 2018. https://doi.org/10.1061/(ASCE)CF.1943-5509.0001183

[8] X. W. Ye, Y. H. Su, and P. S. Han, "Statistical analysis and probabilistic modeling of wim monitoring data of an instrumented arch bridge," *Smart Struct. Syst.*, vol. 17, no. 6, 2016. https://doi.org/10.12989/sss.2016.17.6.1087

[9] Z. Q. Chen, M. G. Liu, X. G. Hua, and T. M. Mou, "Flutter, galloping, and vortex-induced vibrations of H-section hangers," *J. Bridge Eng.*, vol. 17, no. 3, 2012. https://doi.org/10.1061/(ASCE)BE.1943-5592.0000268

[10] Y. L. Ding, Y. H. An, and C. Wang, "Field monitoring of the train-induced hanger vibration in a high-speed railway steel arch bridge," *Smart Struct. Syst.*, vol. 17, no. 6, 2016. https://doi.org/10.12989/sss.2016.17.6.1107

[11] K. Shterev and S. Stefanov, "Strouhal number analysis for a karman vortex gas flow past a square in a microchannel at low mach number," *AIP Conf. Proc.*, vol. 1629, no. 1, p. 319, 2015. https://doi.org/10.1063/1.4902288

[12] H. Ruscheweyh, "Practical experiences with wind-induced vibrations," *J. Wind Eng. Ind. Aerodyn.*, vol. 33, no. 1–2, pp. 211–218, 1990. https://doi.org/10.1016/0167-6105(90)90036-C

[13] S. P. Timoshenko, *History of Strength of Materials: With a Brief Account of the History of Theory of Elasticity and Theory of Structures*. Chelmsford: Courier Corporation, 1983.

[14] Y. Q. Ni, X. W. Ye, and J. M. Ko, "Monitoring-based fatigue reliability assessment of steel bridges: Analytical model and application," *J. Struct. Eng.*, 2010. https://doi.org/10.1061/(ASCE)ST.1943-541X.0000250

[15] X. W. Ye, Y. H. Su, T. Jin, B. Chen, and J. P. Han, "Master S-N curve-based fatigue life assessment of steel bridges using finite element model and field monitoring data," *Int. J. Struct. Stab. Dyn.*, vol. 19, p. S0219455419400133, 2018. https://doi.org/10.1142/S0219455419400133

[16] X. W. Ye, Y. H. Su, P. S. Xi, B. Chen, and J. P. Han, "Statistical analysis and probabilistic modeling of WIM monitoring data of an instrumented arch bridge," *Smart Struct. Syst.*, vol. 17, no. 6, pp. 1087–1105, 2016. https://doi.org/10.12989/sss.2016.17.6.1087

[17] X. W. Ye, Y. Q. Ni, K. Y. Wong, and J. M. Ko, "Statistical analysis of stress spectra for fatigue life assessment of steel bridges with structural health monitoring data," *Eng. Struct.*, vol. 45, 2012. https://doi.org/10.1016/j.engstruct.2012.06.016

[18] British Standard Institution, *BS5400 Part10: Code of Practice for Fatigue*. London: British Standard Institution, 1980.

[19] American Association of State Highways and Transportation Officials, *AASHTO LRFD Bridge Design Specifications*, 2004.

[20] EN1993-2:2006, *Design of Steel Structures Part2: Steel Bridges*, 2006.

[21] J. Kim, "Fatigue assessment of tilting bogie frame for korean tilting train: Analysis and static tests," *Eng. Fail. Anal.*, vol. 13, no. 8, pp. 1326–1337, 2005. https://doi.org/10.1016/j.engfailanal.2005.10.007

[22] H. Li, Z. Zhou, S. Liu, L. Wei, J. Zhao, and H. Su, "Study on fatigue performance of 2200 MPa high-strength wire of main cables based on FE-SAFE," *Coatings*, vol. 13, no. 3, p. 646, 2023. https://doi.org/10.3390/coatings13030646

[23] S. H. Maryam, M. Fidelis, and M. Olivia, "Fatigue performance of bolted shear connectors," *Aust. J. Struct. Eng.*, vol. 23, no. 1, pp. 59–74, 2022. https://doi.org/10.1080/13287982.2021.1999010

[24] D. Veronika, S. Radek, P. Zdeněk, R. Pavel, and K. Adam, "The mechanical properties and fatigue prediction of a new generation of osteosynthesis devices," *Strojnícky časopis - J. Mech. Eng.*, vol. 71, no. 2, pp. 101–108, 2021. https://doi.org/10.2478/scjme-2021-0021

[25] Z. M. Mohammed, F. E. Jihan, and E. A. Awadh, "Fatigue life analysis of laminated elastomeric bearing pad," *Mater. Today Proc.*, vol. 42, no. P5, pp. 2361–2368, 2021. https://doi.org/10.1016/j.matpr.2020.12.328

[26] M. Chen, X. Xiong, W. Zhuang, and F. Zeng, "Fatigue life analysis of automotive glass regulator based on ABAQUS and FE-SAFE," *IOP Conf. Ser.: Earth Environ. Sci.*, vol. 571, no. 1, p. 012109, 2020. https://doi.org/10.1088/1755-1315/571/1/012109

[27] Q. Zheng, N. Wang, P. Zhu, J. Liu, and W. Ma, "Fatigue life simulation and analysis of aluminum alloy sheet self-piercing riveting," *Fract. Struct. Integr.*, vol. 14, no. 53, pp. 141–151, 2020. https://doi.org/10.3221/IGF-ESIS.53.12

[28] H. Xiao, X. Guo, H. Y. Wang, X. Ling, and S. X. Wu, "Fatigue damage analysis and life prediction of e-clip in railway fasteners based on ABAQUS and FE-SAFE," *Adv. Mech. Eng.*, vol. 10, no. 3, p. 168781401876724, 2018. https://doi.org/10.1177/1687814018767249

[29] P. A. Seaburg and C. J. Carter, *Steel Design Guide 9: Torsional Analysis of Structural Steel Members*, 2nd ed. Chicago: AISC, 2003.

[30] P. Keller, "Wind induced torsional fatigue behavior of truss bridge verticals," Master's thesis, Oregon State University, 2012.